Available online at www.sciencedirect.com
ScienceDirect
Thermochimica Acta 464 (2007) 42–58
thermochimica acta
www.elsevier.com/locate/tca

Liquid state thermochemical decomposition of neat 1,3,5,5-tetranitrohexahydropyrimidine (DNNC) and its DNNC-d_2, DNNC-d_4, DNNC-d_6 structural isotopomers: Mechanistic entrance into the DNNC molecule☆,☆☆

S.A. Shackelford[a,b,*], J.A. Menapace[b], J.F. Goldman[c]

[a] *Air Force Research Laboratory, Propellants Branch (AFRL/PRSP), 10 East Saturn Blvd., Edwards AFB, CA 93524-7680, USA*
[b] *Directorate of Chemical Sciences, FJSRL, USAF Academy CO, USA*
[c] *Department of Chemistry, USAF Academy, CO, USA*

Received 18 June 2007; accepted 4 August 2007
Available online 19 August 2007

Abstract

Global kinetics for the liquid state thermochemical decomposition of neat 1,3,5,5-tetranitrohexahydropyrimidine (DNNC), perdeuterio-labeled DNNC-d_6, and partially deuterium-labeled DNNC-d_2 and DNNC-d_4 isotopomers were obtained by isothermal differential scanning calorimetry (IDSC). Molecular kinetic deuterium isotope effect (KDIE) values obtained with DNNC and DNNC-d_6 from 174 to 194 °C revealed that C–H bond rupture regulates both an endothermic catalytic initiation and the exothermic propagation of the liquid thermochemical decomposition process. Using IDSC-based KDIE comparisons with the DNNC-d_2, DNNC-d_4, and DNNC-d_6 isotopomers, a more detailed chemical structure/mechanistic relationship emerged by entering the interior of the DNNC molecule. Here structural kinetic KDIE results showed the rate-controlling C–H bond rupture has its origin at the non-equivalent C-2 methylene group sandwiched between the two nitrated DNNC nitrogen ring atoms, versus at the chemically equivalent C-4 and C-6 methylene ring positions located elsewhere in the DNNC molecule. Elucidation of such mechanistic features should aid in the structural design of new high-energy compounds with improved thermochemical properties. A 170.0 kJ/mol activation energy appeared for the endothermic induction period, and a lower 104.2 kJ/mol activation energy was determined for the exothermic acceleratory portion of the DNNC decomposition process. The global liquid and solid state thermochemical decomposition processes for DNNC are compared.
Published by Elsevier B.V.

Keywords: 1,3,5,5-Tetranitrohexahydropyrimidine; DNNC; Liquid state decomposition; Deuterium isotope effect; KDIE

1. Introduction

Although complex global reaction kinetics, obtained by relatively inexpensive thermal analysis methods, often are ignored in favor of highly defined individual kinetic steps requiring more sophisticated and expensive equipment [1], global kinetics data can describe complex thermochemical decomposition processes in ways which critically impact practical technology and safety concerns [1,2]. For example, isothermal differential scanning calorimetry (IDSC) global kinetics rate constants, determined for the solid state thermochemical decomposition of 1,3,5-triamino-2,4,6-trinitrobenzene (TATB), accurately predict the 354 °C experimentally determined critical temperature which initiates a thermal explosion event [3].

The condensed phase neat thermochemical decomposition process an energetic compound follows is primarily a complex mechanistic set of interacting intermolecular bimolecular reactions [4] with some degree of intramolecular unimolecular character. Generally, two key chemical bond ruptures occur

☆ Portions of this material were presented at the following conferences: 35th International Conference of ICT: Energetic Materials, Structure and Properties, Karlsruhe, Germany, June 29–July 2, 2004; 203rd Nat. Am. Chem. Soc. Mtg., San Francisco, CA, USA, April 5–10, 1992; and 22nd International Conference of ICT: Combustion and Reaction Kinetics, Karlsruhe, Germany, July 2–5, 1991.

☆☆ Experimental IDSC thermochemical decomposition investigations were conducted at The F.J. Seiler Research Laboratory (FJSRL), USAF Academy, CO, USA prior to its September 30, 1995 decommissioning.

* Corresponding author. Tel.: +1 661 275 5847; fax: +1 661 275 5471.
E-mail address: scott.shackelford@edwards.af.mil (S.A. Shackelford).

0040-6031/$ – see front matter. Published by Elsevier B.V.
doi:10.1016/j.tca.2007.08.005

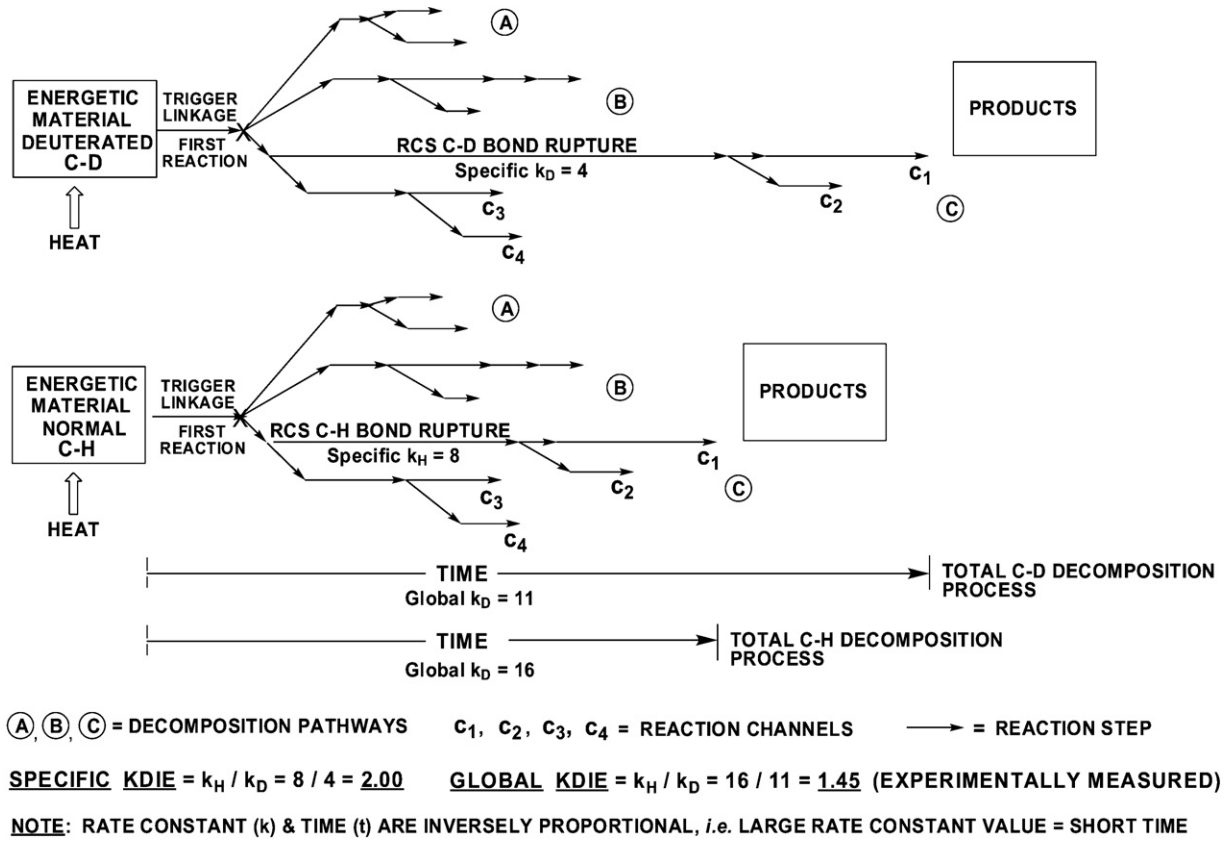

Fig. 1. General thermochemical decomposition process schematic representation and the KDIE measurement context [13].

during the thermochemical decomposition process, the initial bond rupture and the rate-controlling bond rupture; rarely does one bond rupture constitute both. The first is the initial homolytic bond rupture (scission or cleavage) which determines the specific pathway (e.g. A, B, or C in Fig. 1) the decomposition process will follow and the resultant product composition. Certain structural arrangements in an energetic molecule (e.g. N–NO_2 for secondary nitramines) [5] are reaction centers (explosophores) [6] for this initial bond rupture which often are termed the "trigger linkage," or more recently, the "first reaction" [7]. Once this specific pathway is established (pathway C in Fig. 1), a myriad of subsequent chemical reaction channels proceed which occur in series and competing parallel sequences. Along this reaction pathway, one individual chemical reaction in a specific reaction channel proceeds more slowly than all others (longest arrow) where individual reaction steps are represented as arrows (Fig. 1). It is during this slowest reaction step that the second critical homolytic bond rupture occurs which significantly regulates the overall rate at which this slowest reaction channel and the entire decomposition process proceeds. This subsequent KDIE-determined rate-controlling chemical bond rupture, accompanied by a concomitant atom transfer [8], occurs early in the thermochemical decomposition process [2,8–10] and usually is not synonymous with the trigger linkage, but closely follows it. This rate-controlling bond rupture can be determined *in situ* using the kinetic deuterium isotope effect (KDIE) approach in conjunction with ambient pressure isothermal DSC [2,3,8–11], reaction quenching [11], or TGA [12] analyses. If this slowest reaction did not exert a significant impact on the overall global decomposition rate, a noticeable global KDIE would not be observed. In the example illustrated by Fig. 1, note that the slow individual rate-controlling reaction step rate for either the normal energetic compound or its deuterium-labeled analogue cannot be measured in isolation where a specific KDIE = 2.00 would be determined. Rather, the entire global decomposition process must be analyzed, and the overall rates for the energetic compound and its deuterated analogue are compared when determining a KDIE value [13]. Thus, the measured global KDIE value (1.45) is likely a smaller number than what would be found for the specific KDIE value (2.00) in the individual rate-controlling step.

This critical rate-controlling bond rupture has been determined for the ambient pressure thermochemical decomposition processes of TNT [10], TATB [3], HMX [8,12], and RDX [11,12]. In every case, the same mechanistic rate-controlling bond rupture found in the ambient pressure decomposition process for each compound, proved to be a significant rate-controlling mechanistic feature observed in rapid deflagration [8,14], high-pressure combustion [14–16], and thermal explosion events [3,14]. Furthermore, it is detected as being a significant contributing mechanistic feature in impact or shock explosive initiation sensitivity [12,17–23]. Identification of the pathway directing initial bond rupture, of the subsequent rate-controlling bond rupture, and of the resultant product composition formed during the thermochemical decomposition processes are critical for obtaining energetic compounds

with improved thermochemical and initiation sensitivity properties.

The first KDIE approach applied to the thermochemical decomposition of an energetic compound occurred with neat liquid TNT and TNT-α-d_3 [10]. IDSC analysis during the TNT endothermic induction period, the earliest portion in the thermochemical decomposition process, revealed that C–H bond rupture in the pendant TNT methyl group controls the formation of a catalytic species, which upon reaching a minute threshold concentration, initiates the TNT exothermic acceleratory phase and a concomitant energy release. A subsequent KDIE study with solid state TATB and TATB-d_6 found that N–H bond rupture also constituted the rate-controlling mechanistic feature early during the thermochemical decomposition process [3].

The seminal KDIE-based thermochemical decomposition investigation of a heterocyclic nitramine was accomplished with HMX and HMX-d_8 and revealed a different KDIE and rate-controlling mechanistic step dependence on the HMX physical state [8]. This IDSC study showed a rate-controlling C–H bond rupture occurred during solid state decomposition along with other rate-controlling features in the mixed-melt and liquid state decompositions. Proposed was an initial N–NO_2 bond rupture to form the NO_2 radical which then, either, unimolecularly from an HMX radical intermediate existing in a proposed cage effect [24], or bimolecularly from a neutral HMX molecule, transfers a hydrogen atom via NO_2 radical abstraction to form the unstable HONO species [8]. This unstable species undergoes further decomposition to form other oxidizing and catalytic species [8], such as NO, NO_2, and H_2O, or in some cases, possibly OH and NO [25], while resultant HMX radicals continue along various decomposition reaction channels and condensed phases [8].

This rate-controlling C–H bond rupture for solid state HMX was confirmed by a subsequent HMX/HMX-d_8 isothermal TGA decomposition study [12]. Later, a more detailed mechanistic isothermal pyrolysis investigation with HMX and HMX-d_8 was conducted using simultaneous thermogravimetric modulated beam mass spectrometry (STMBMS) where different reaction channels of specific product specie formation, during the decomposition process, could be measured concurrently [26,27]. At least four different reaction channels were identified, and a large KDIE was found for water product formation. Finding a large KDIE for water formation also was consistent with an initial N–NO_2 bond cleavage, a subsequent rate-controlling methylene C–H bond rupture and hydrogen atom transfer from an HMX species to form the unstable HONO molecule [8] and its decomposition to the water byproduct. Water, occluded in the HMX crystal structure, also was suggested as a hydrogen atom donating catalyst for another reaction channel [27]. Conceivably, the water product, formed via the KDIE measured rate-controlling C–H bond rupture outlined above, also could contribute to the water catalysis channel.

The same rate-controlling C–H bond rupture was identified for the liquid state thermochemical decomposition of RDX and RDX-d_6 using isothermal TGA [12] This result was further verified by a subsequent IDSC and a UV-based reaction quenching

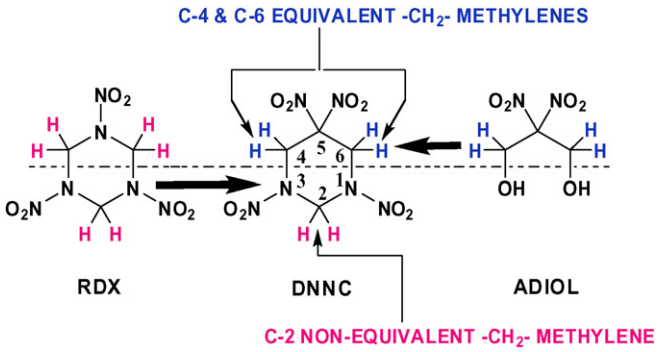

Fig. 2. Unique hybrid chemical structure of the DNNC molecule.

KDIE study [11]. A later STMBMS RDX/RDX-d_6 investigation revealed a complex multi-channeled liquid thermochemical decomposition process which was different from HMX, but still revealed a rate-controlling C–H bond rupture, and atom transfer from the RDX methylene group, both being highly prevalent mechanistic features [25,28,29]. In fact, it appears the progression rate of all four reaction channels may depend upon C–H bond rupture in the first channel.

While much more thermally stable than the RDX, the cyclic DNNC nitramine derivative (Fig. 2) undergoes extensive solid state thermochemical decomposition during long-term exposure in the 142–148 °C temperature range [2]. IDSC-based KDIE results suggest that ring C–N bond rupture for the solid state decomposition likely is the rate-controlling bond rupture during the long endothermic induction period, wherein a catalytic species likely forms, and upon reaching a threshold concentration, initiates an autocatalytic exothermic acceleratory phase. Once the acceleratory phase is initiated, C–H bond rupture is the rate-controlling mechanistic feature which regulates its energy release rate. The endothermic induction period for the solid state decomposition process has a higher activation energy of 128 kJ/mol compared to the 115–106 kJ/mol [2,30] determined for the exothermic acceleratory phase. This supports the likely formation of a catalytic species from the DNNC molecule during the solid state induction period and mirrors the thermochemical behavior followed by the neat liquid TNT thermochemical decomposition process [10].

The relationship of the mechanistic rate-controlling homolytic bond rupture found in ambient pressure thermochemical decomposition processes to higher temperature, higher pressure catastrophic events such as deflagration, combustion, thermal explosion, detonation, and to energetic compound sensitivity issues, is well documented [9,13,14,23]. Given the importance of this high-energy rate-controlling mechanistic feature, the thermochemical decomposition of neat liquid DNNC, and its three isotopomers, DNNC-d_6, DNNC-d_4, and DNNC-d_2, was investigated by isothermal DSC to determine the rate-controlling homolytic bond rupture and its location in the DNNC molecular structure. Similarities and differences between this neat liquid state DNNC thermochemical decomposition process, and the previously reported mechanistic solid state DNNC thermochemical decomposition investigation [2], also are compared.

2. Experimental

Caution! Although reasonably stable to accidental explosive initiation, DNNC is a high-energy explosive material. Care should be taken to use proper laboratory shielding and safety procedures in all handling and transfer operations.

2.1. Isothermal DSC analysis

All isothermal DSC measurements were made with a Perkin-Elmer DSC 7 instrument described previously [2] using DNNC sample sizes ranging from 1.50 to 1.53 mg. Prior to conducting the thermochemical decomposition runs, the DSC 7 temperature was calibrated at a 1 K/min scanning rate using a two-temperature calibration procedure with indium (m.p. 156.60 °C) and tin (231.88 °C) standards. The temperature of the DNNC sample (m.p. = 154.8–156.2 °C) [31] was stabilized to 30 °C under the nitrogen gas atmosphere and then was brought to its pre-determined isothermal decomposition temperature (174, 178, 182, 186, 190, or 194 °C) at a 480 °C per minute heating rate.

2.2. Isothermal DSC data reduction

The length of the endothermic induction period, and resultant induction times, were visually determined from individual thermograms generated for each IDSC run. The minute units were then converted to seconds for the calculations used to obtain activation energy and KDIE values. For determining the exothermic acceleratory phase rate constants, software programs were written at our laboratory to transfer the data from each designated IDSC run to a separate PC station, and then, to input the data into an autocatalytic kinetics plot program that used the $\delta\alpha/\delta t = k\alpha(1-\alpha)$ autocatalytic rate equation, where α is the mole fraction of decomposed DNNC at any given time (t). A software program, based on that developed at the Los Alamos National Laboratory [32], was used and is described in detail elsewhere [2,8].

2.3. Synthesis of DNNC and the DNNC-d_6, DNNC-d_4, and DNNC-d_2 structural isotopomers

The synthesis of ADIOL and ADIOL-d_4 (2,2-dinitropropane-1,3-diol-1,1,3,3-d_4) reactants, needed to obtain DNNC and its DNNC-d_6 analogue, was previously described [33]. The partially deuterium-labeled DNNC-d_2 and DNNC-d_4 compounds were synthesized using an identical Mannich condensation reaction procedure, and scaled as needed, by employing the appropriate choice of unlabeled or deuterium-labeled 2,2-dinitropropane-1,3-diol (ADIOL and ADIOL-d_4) and formaldehyde or formaldehyde-d_2, plus unlabeled *tert*-butylamine in methanol solvent. These initial Mannich condensation reactions provided the DBNP-d_2 and DBNP-d_4 intermediate compounds which were then converted to their respective final DNNC-d_2 and DNNC-d_4 products by 100% anhydrous nitric acid nitration. All ^{1}H NMR (acetone-d_6, TMS std.), mass spectral, FTIR (Kubelka/Munk) powder analyses and melting points for DBNP-d_2, DBNP-d_4, DNNC-d_2 (155–157 °C), and DNNC-d_4 (155–156 °C) were consistent when compared with previously reported values for the unlabeled DBNP, and DNNC analogues [33]. Yields obtained for DBNP-d_2 and DBNP-d_4 compounds were similar to DBNP (75%) and DBNP-d_6 (72%). Final product yields for DNNC-d_2 (63%) and DNNC-d_4 (75%) compared well with DNNC (72%) and DNNC-d_6 (71%) [33]. Within the accuracy and precision of ^{1}H NMR integration values, the intermediate DBNP-d_2 reflected an incorporation of 2.2 methylene deuterium atoms; DBNP-d_4 incorporated 4.0 methylene deuterium atoms, and 5.9 methylene deuterium atoms were incorporated into the DBNP-d_6 molecule relative to the two unlabeled *tert*-butyl groups substituted on the ring nitrogen atoms at the 1- and 3-ring positions. Because of the synthesis method used [33], the $-CD_2-$ labeled methylenes were incorporated into the DNNC ring structure as a discreet unit; mixed $-CHD-$ methylenes could not form. Proton NMR integrations of the two different methylene groups (δ 6.30 C-2 and δ 5.47 C-4 and C-6) for both DNNC-d_4 and DNNC-d_2 remained in a 1:2 integration ratio, respectively, indicating a random distribution of the labeled $-CD_2-$ deuterium-labeled methylene groups occurred at all three C-2, C-4, and C-6 ring positions. In spite of this randomized $-CD_2-$ methylene distribution, relevant mechanistic information was obtained by comparing DNNC, DNNC-d_2, DNNC-d_4, and DNNC-d_6 IDSC isotopomer induction times and rate constants.

3. Results and discussion

The initial homolytic bond rupture of an energetic material controls the reaction pathway, the number of reaction channels, the decomposition products, and the product composition of a thermochemical decomposition process. Later rate-controlling homolytic bond rupture ultimately controls the overall energy release rate during the decomposition of a given energetic material. Improved thermochemical properties must start with decreasing the rate at which a decomposition process proceeds, either kinetically, or by chemical structure alteration. An excellent example of possible progress is found in the chemical structure similarity and differences which exist between the symmetrical RDX cyclic nitramine molecule and the unsymmetrical DNNC cyclic pseudo-nitramine (Fig. 2). This led us to investigate the solid and liquid state decomposition of 1,3,5,5-tetranitrohexahydropyrimidine (DNNC) pseudo-nitramine [2,30] for comparison with RDX.

First synthesized in 1984 [34–36], the DNNC molecule, is a unique heterocyclic hybrid structure which contains structural features found in both saturated cyclic nitramines (RDX and HMX) and in aliphatic geminal-dinitroalkyl compounds (Fig. 2). While RDX contains three chemically equivalent ($-CH_2-$) methylenes, the DNNC structural variation provides three methylene ($-CH_2-$) groups where only two are chemically equivalent. Of the three DNNC methylenes situated at the C-2, C-4, and C-6 positions, the two methylene groups at the C-4, and C-6 positions, adjacent to the geminal dinitro-substituted C-5 carbon [$-C(NO_2)_2-$], are in a chemically equivalent envi-

ronment like that found in RDX, but the third DNNC methylene group at the C-2 position, sandwiched between the two nitrated ring N atoms (=NNO_2), is chemically non-equivalent with respect to the C-4 and C-6 methylene positions.

Because of this structural variation, DNNC thermochemical stability resembles that of TNT, rather than its structurally related RDX and HMX nitramines, but does provide an explosive energy output which rivals RDX [2,33]. Like TNT (m.p. = 80.0–81.2 °C) [10], neat DNNC melts without noticeable decomposition when heated above its 154.8–156.2 °C melting point; thus, a 5.19 kcal/mol (21.72 kJ/mol) DNNC heat of fusion could be determined by DSC analysis [31] (TNT ΔH_{fusion} = 5.34 kcal/mol or 22.34 kJ/mol) [37]. Related cyclic nitramines RDX and HMX melt, or undergo liquefaction, with decomposition rapidly enough that their heat of fusion cannot be obtained. Additionally, DNNC and RDX structural variation affects thermochemical properties related to rapid pyrolysis and simulated combustion behavior [4,38].

The liquid state thermochemical decomposition process for both DNNC and DNNC-d_6 was conducted at 4 °C temperature intervals from 174 to 194 °C using isothermal differential scanning calorimetry (IDSC). Each DNNC and DNNC-d_6 IDSC run provided a thermogram curve displaying three main features: (1) an endothermic induction period, (2) followed by the initiation of an exothermic acceleratory phase which, after reaching a maximum energy release at the thermogram peak, (3) entered into a decreasing exothermic decay phase until complete decomposition resulted. Ample thermogram curve shifts between each IDSC thermogram were obtained at the six isothermal temperatures (174, 178, 182, 186, 190, and 194 °C) selected for relevant kinetic evaluation (Fig. 3).

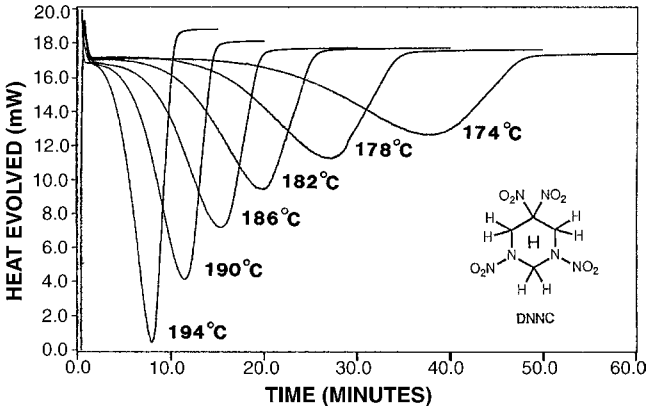

Fig. 3. Individual IDSC thermograms of DNNC from 174 to 194 °C taken at 4 °C intervals.

3.1. Thermochemical physical and kinetic properties

Within this 20 °C temperature regime (174–194 °C), post IDSC sample weights of decomposed neat liquid DNNC showed an average 81% mass loss from conversion to gaseous products (Table 1). The remaining 19% of the DNNC sample was converted to solid phase residue product(s) and remained in the sample pan. The liquid DNNC-d_6 decomposition process gave a nearly identical weight loss average of 80% with a 20% solid phase residue (Table 2). For comparison, solid state DNNC thermochemical decomposition afforded a 76% mass loss and solid state DNNC-d_6 a slightly smaller 73% mass decrease. Formation of a solid phase residue has very important implications in IDSC kinetic data evaluation.

Table 1
Physical and kinetic properties of neat liquid DNNC thermochemical decomposition

Temperature (°C)	Induction time (s)	Rate constant ($k \times 10^{-3}$ s^{-1})	k linearity (%)[a]	$\Delta H_{decomp.}$ (kJ/mol)	Wt. loss (%)	No. runs
194	52.6 ± 28.3	12.15 ± 0.48	68	−802.5 ± 48.5	80 ± 2	8
190	72.2 ± 19.3	9.61 ± 0.43	83	−775.3 ± 56.9	82 ± 4	5
186	93.8 ± 17.5	7.55 ± 0.64	94	−801.6 ± 30.1	82 ± 4	5
182	148.4 ± 13.8	5.87 ± 0.39	95	−786.6 ± 38.1	80 ± 5	5
178	228.6 ± 76.4	4.58 ± 0.25	94	−799.1 ± 61.1	80 ± 7	5
174	359.6 ± 153.7	3.45 ± 0.16	95	−803.3 ± 38.1	80 ± 3	5
Average	–	–	–	−795.0 ± 45.6	81 ± 4	–

All data variances computed at the 99% Student t level.
[a] Percent of thermogram exothermic acceleratory phase fitting linear portion of the autocatalytic rate plot at a 0.999 least squares value (R^2).

Table 2
Physical and kinetic properties of neat liquid DNNC-d_6 thermochemical decomposition

Temperature (°C)	Induction time (s)	Rate constant ($k \times 10^{-3}$ s^{-1})	k linearity (%)[a]	$\Delta H_{decomp.}$ (kJ/mol)	Wt. loss (%)	No. runs
194	73.6 ± 35.1	7.16 ± 0.89	57	−766.5 ± 36.4	80 ± 3	6
190	126.5 ± 28.3	5.94 ± 0.45	72	−797.9 ± 119.7	84 ± 12	5
186	169.9 ± 39.5	4.71 ± 0.35	81	−777.8 ± 81.2	81 ± 4	6
182	274.0 ± 59.6	3.58 ± 0.19	82	−767.8 ± 53.3	81 ± 6	5
178	437.4 ± 120.6	2.76 ± 0.29	82	−754.8 ± 25.1	81 ± 4	5
172	652.0 ± 82.2	2.06 ± 0.10	83	−769.0 ± 24.3	77 ± 1	5
Average value	–	–	–	−772.4 ± 56.9	80 ± 5	–

All data variances computed at the 99% Student t level.
[a] Percent of thermogram exothermic acceleratory phase fitting linear portion of the autocatalytic rate plot at a 0.999 least squares value (R^2).

Post solid phase residue can mean that intermediate derivatives form during the thermochemical decomposition process which react further until decomposition is complete. Two problems can result, and both can cause a misinterpretation of the KDIE value and its associated kinetics. First, kinetic evaluation may provide a combined rate constant value to which decomposition of the subject compound and further decomposition of the intermediate condensed phase derivatives both contribute. This results in a KDIE value which is diluted or reduced from the true value of the subject compound. Secondly, this rate constant may reflect data from decomposition of the condensed phase derivatives only formed from the initial energetic compound. In this case, the KDIE value offers no useful information about the original energetic compound and its decomposition process. These two related problems are amply documented in IDSC thermochemical decomposition investigations with liquid TNT [9,10] and solid TATB [3,9]. When the presence of condensed phase products appear, only the early portion of the thermochemical decomposition process, and the corresponding thermogram portion, should be evaluated, notably, the endothermic induction period and the exothermic acceleratory phase.

The DNNC and DNNC-d_6 thermochemical decomposition process afforded smooth thermograms that followed an autocatalytic rate behavior during a large portion of the exothermic acceleratory phase (Fig. 3). The obvious incremental rate increase as one proceeds to higher temperatures, is visually depicted with decreasing induction times (t_i) and steeper (faster) acceleratory phase portions reflecting a higher rate constant (k). The percent of the acceleratory phase that could be fitted linearly to the autocatalytic rate plot, the exceptional least squares linear curve fits (R^2) obtained, and the corresponding rate constants (k) determined from the slopes of the linear portion of the autocatalytic rate plot at each temperature, are found in Table 1. The rate constants shown at each isothermal temperature are averaged over at least five runs. Fig. 4 illustrates the conversion of one thermogram run at 182 °C into its autocatalytic rate plot. Analogous data for DNNC-d_6 appear in Table 2. At a liberal 99% Student t variation analysis, each rate constant is unique and does not overlap with ones at adjacent temperatures. The heat of decomposition for both DNNC and DNNC-d_6 give similar values.

Compared to the solid state DNNC thermochemical decomposition process [2], both the induction period and acceleratory phase kinetics proceed much faster above the 154.8–156.2 °C DNNC melting point. For example, the 184 min (11,040 s) induction time for solid state DNNC at 148 °C is nearly 7.5 times longer than the 148 s for liquid state DNNC at 182 °C. For the liquid state DNNC acceleratory phase at 182 °C, the rate constant seen in Table 1 is slightly over one order magnitude faster than the 3.38×10^{-4} s^{-1} rate constant obtained at 148 °C for solid state DNNC [2]. The liquid state DNNC thermochemical decomposition releases heat energy much more rapidly than does the solid state process.

Activation energies, computed at a 95% Excel©standard error level, reveal a 170.0 ± 27.7 kJ/mol energy of activation ($R^2 = 0.9922$) for the DNNC induction period using the five lower temperatures from 174 to 190 °C (Fig. 5). At higher

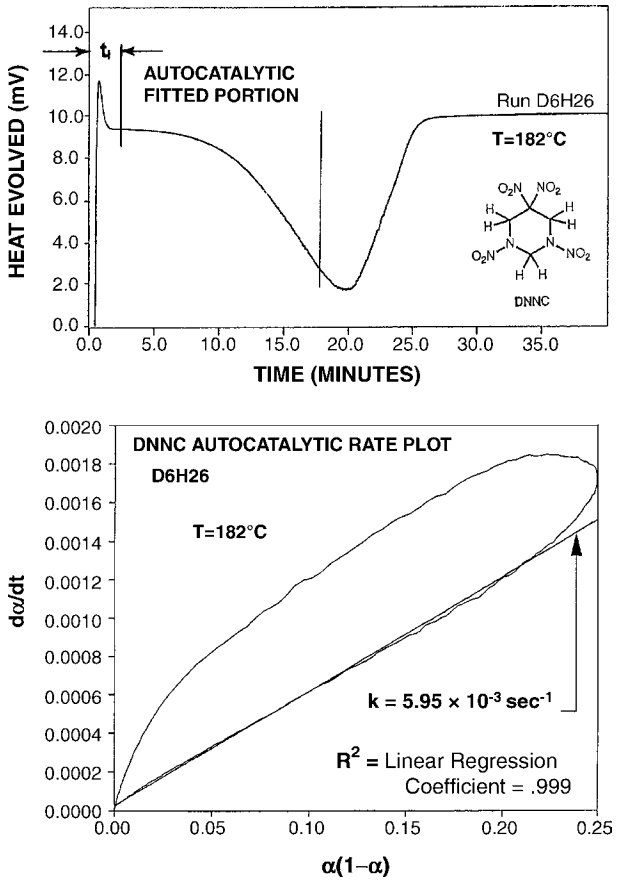

Fig. 4. (top) DNNC isothermal DSC thermogram (Run D6H26) illustrating the portion of the exothermic acceleratory phase that fits autocatalytic kinetics following the endothermic induction period (t_i). (bottom) Corresponding autocatalytic rate plot for DNNC (Run D6H26) illustrating the linear kinetic fit of the exothermic acceleratory phase and slope-determined rate constant (k).

temperatures, the induction period time is short enough that it approaches the instrumental temperature equilibration regime, and accurate measurement becomes difficult. Little time is left for a linear induction period portion in the thermogram curve to develop, and this can mask the point of curve deflection where the acceleratory phase is initiated. An induction period activation energy, which includes all six temperatures, equals 160.5 kJ/mol

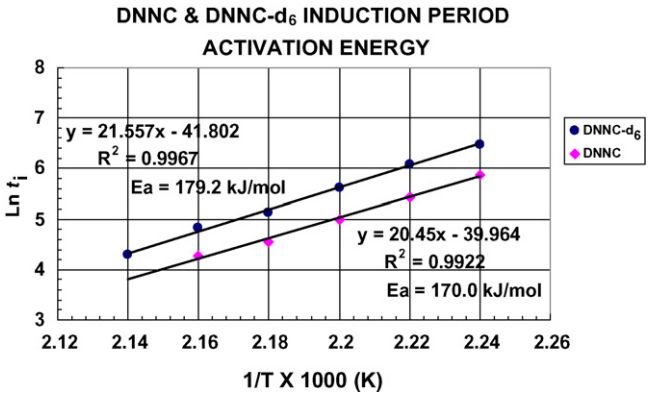

Fig. 5. Kinetic data plot providing the activation energy for the DNNC endothermic induction period.

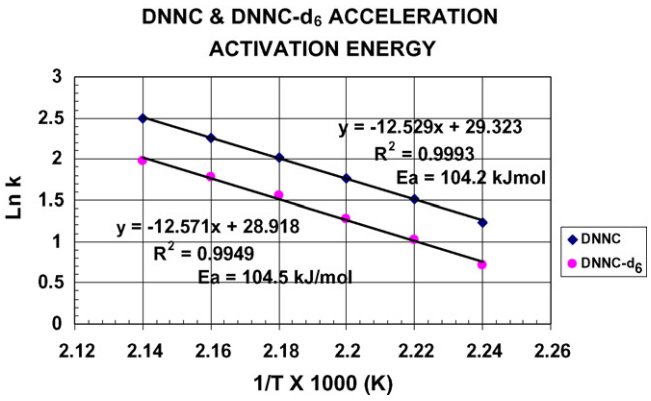

Fig. 6. Kinetic data plot for activation energy of the DNNC and DNNC-d_6 exothermic acceleratory phase.

but gives a less desirable linear curve fit ($R^2 = 0.9903$); therefore, the higher 170.0 kJ/mol is selected as more valid. The 170 kJ/mol graphic plot uses, as the shortest induction time, a 72.2 s value determined at 190 °C which is in the same time regime as that of the shortest DNNC-d_6 induction time value (73.6 s) at the higher 194 °C temperature.

A noticeably lower 104.2 ± 3.9 kJ/mol energy of activation is found for the DNNC exothermic acceleratory phase. Using the rate constant values for all six temperatures, an excellent linear data fit results ($R^2 = 0.9993$) as seen in Fig. 6. The significantly lower 65.8 kJ/mol energy of activation (170.0–104.2 kJ/mol) for the exothermic acceleratory phase follows the same trend as that seen for the solid state DNNC thermochemical decomposition process [2]. This trend suggests the possible formation of a small amount of decomposition product from DNNC itself during the endothermic induction period, which, upon reaching a threshold concentration, catalyzes initiation of the autocatalytic exothermic acceleratory phase where DNNC releases its stored energy. This lower energy of activation and autocatalytic decomposition process for the exothermic acceleratory phase of liquid state DNNC fits with catalytic behavior. It also mirrors the same pattern as that seen for the solid state DNNC decomposition process [2], as well as that reported for the neat liquid TNT catalyzed decomposition process [10].

Because significantly slower kinetics result with DNNC-d_6, induction times are longer at corresponding temperatures used with DNNC; so, all six temperatures are included to obtain the 179.2 ± 14.3 kJ/mol ($R^2 = 0.9967$) induction period activation energy (Fig. 5). The same activation energy trend was determined for the neat liquid state DNNC-d_6 thermochemical decomposition process (Table 3). The DNNC-d_6 rate constants at corresponding temperatures are significantly lower than those for DNNC and reflect the presence of a positive kinetic deuterium isotope effect (KDIE). As with the DNNC thermochemical decomposition process, a large portion of the DNNC-d_6 exothermic acceleratory phase provides an excellent $R^2 = 0.999$ linear fit with the autocatalytic rate plot. A noticeably lower 104.5 ± 10.4 kJ/mol activation energy ($R^2 = 0.9949$) also was observed for the DNNC-d_6 acceleratory phase (Fig. 6) compared to its induction period (Fig. 5). For both DNNC and DNNC-d_6, the higher induction period activation energy is statistically significant even at a most strenuous 99% variance level (Table 3).

Activation energy (E_{act}) comparisons for solid and liquid state DNNC thermochemical decomposition also are shown in Table 3. While DNNC is considered to be a thermally stable compound, given enough time and energy, solid state DNNC proceeds through a slow thermochemical decomposition process and, like its liquid phase decomposition process, proceeds with an induction period activation energy that is higher than that seen for the acceleratory phase.

3.2. Molecular kinetic deuterium isotope effect

The molecular KDIE for a given compound is determined by comparing thermochemical decomposition rates of the unlabeled molecule (DNNC) with the perdeuterio-labeled molecule (DNNC-d_6). Comparing both induction period and acceleratory phase data at the same temperatures in Tables 1 and 2, shows that the non-isotopically labeled (normal) DNNC thermochemically decomposes more rapidly than its fully deuterium-labeled DNNC-d_6 analogue. Like that previously reported for liquid TNT [10], solid TATB [3], solid and liquid HMX [8,12], solid and liquid RDX [11,12], and solid DNNC [2], a positive molecular kinetic deuterium isotope effect (KDIE) defines the liquid state DNNC thermochemical decomposition process.

This positive KDIE clearly is observed in Fig. 7 where individual DNNC and DNNC-d_6 thermograms taken at 174 °C are compared. Fig. 8 displays how the magnitude of the KDIE can reveal the specific rate-controlling homolytic bond cleavage associated with the DNNC molecule. Table 4 lists the KDIE values obtained at each temperature using the DNNC and DNNC-d_6 induction periods and the overall KDIE determined for the entire 172–194 °C temperature range. The induction period KDIE is determined by dividing the DNNC-d_6 induction time with the DNNC induction time (t_{id}/t_{ih}) [8–10]. A molecular KDIE value of 1.76 found during the induction period reflects a primary effect and identifies C–H bond rupture in the ring methylene ($-CH_2-$) groups of the DNNC molecule, or a structural fragment derived from it, as being the rate-controlling mechanistic feature (Fig. 8).

Table 3
Activation energy (kJ/mol) comparisons between liquid and solid state DNNC thermochemical decomposition processes

Thermogram portion	Liquid DNNC (R^2)	Liquid DNNC-d_6 (R^2)	Solid DNNC (R^2)	Solid DNNC-d_6 (R^2)
Induction period	170.0 ± 50.8 (0.992)	179.2 ± 23.7 (0.997)	128.1 (0.992) [2]	Not determined
Acceleratory phase	104.2 ± 6.5 (0.999)	104.5 ± 17.2 (0.995)	105.6 (calc.) [2]	115.2 (0.998) [2]

Variances computed at Excel© 99% standard error level.

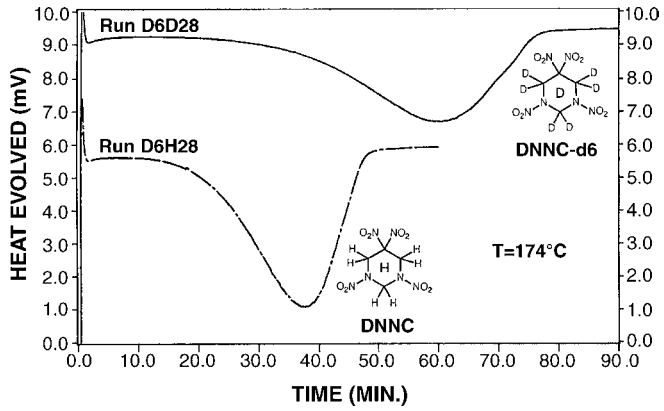

Fig. 7. Individual DNNC and DNNC-d_6 IDSC thermograms compared at 174 °C.

Immediately following the endothermic induction period, the DNNC thermochemical decomposition process enters into an exothermic autocatalytic acceleratory phase. In this portion of the thermogram (Table 5), KDIE behavior is determined by dividing the normal DNNC rate constant by the deuterium-labeled DNNC-d_6 rate constant (k_h/k_d) [8–11]. Within the 174–194 °C temperature range, a substantial overall molecular KDIE equal to 1.65 is found (Table 5). Among the myriad of chemical reaction channels in play during this complex exothermic acceleratory portion of the thermochemical decomposition process, a rate-controlling C–H bond rupture occurs in the substantially slowest one. This C–H bond rupture is derived from the methylene sites of the cyclic DNNC molecule, or a structural fragment derived from it, and significantly controls the overall exothermic energy release rate. This 1.65 KDIE value is calculated to be 3.17 when mathematically normalized to room temperature conditions (298 K) [39] and further verifies assignment of a rate-controlling C–H bond rupture where, at 298 K, a primary KDIE equal to 2.5 is considered to be the minimum [40]. This primary 1.65 KDIE value for the exothermic acceleratory phase decomposition of liquid DNNC is quite similar to that found for the liquid decomposition process of structurally related RDX which was measured using three different analysis methods (Table 6). Rounded off to the nearest tenth decimal place, a 1.6 molecular KDIE value emerges for the exothermic portion of both the liquid state DNNC and RDX thermochemical decomposition processes.

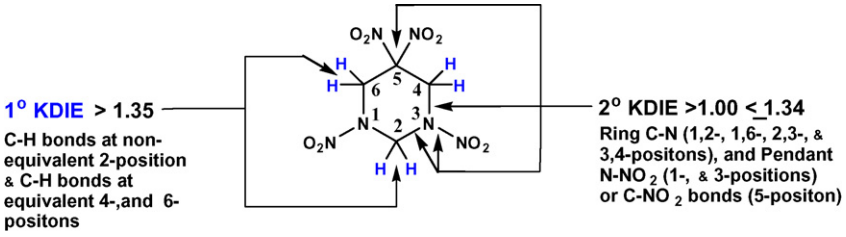

Fig. 8. Possible KDIE types from C—H (1° KDIE) bond rupture and C—N, N—NO_2, C—NO_2 (2° KDIE) potentially present with the DNNC molecular structure.

Table 4
Induction period kinetic deuterium isotope effect (KDIE) for DNNC

Temperature (°C)	DNNC-d_6 induction period (min)	DNNC induction period (min)	KDIE value (no units)
194	1.23 ± 0.53	0.88 ± 0.17	1.40 ± 0.47
190	2.11 ± 0.41	1.20 ± 0.29	1.76 ± 0.32
186	2.83 ± 0.59	1.56 ± 0.41	1.81 ± 0.34
182	4.57 ± 0.89	2.47 ± 0.10	1.85 ± 0.20
178	7.29 ± 1.79	3.81 ± 1.13	1.91 ± 0.38
172	10.87 ± 1.21	5.99 ± 2.29	1.85 ± 0.30
Average	–	–	1.76 ± 0.33

Data variances computed at the 99% Student t level.

Table 5
Acceleratory phase kinetic deuterium isotope effect (KDIE) for DNNC

Temperature (°C)	DNNC rate constant ($k \times 10^{-3}$ s^{-1})	DNNC-d_6 rate constant ($k \times 10^{-3}$ s^{-1})	KDIE expl. value	KDIE at 25 °C [39]
194	12.15 ± 0.48	7.16 ± 0.89	1.70 ± 0.13	3.36
190	9.61 ± 0.43	5.94 ± 0.45	1.62 ± 0.09	3.16
186	7.55 ± 0.64	4.71 ± 0.35	1.60 ± 0.11	3.10
182	5.87 ± 0.39	3.58 ± 0.19	1.64 ± 0.08	3.14
178	4.58 ± 0.25	2.76 ± 0.29	1.66 ± 0.12	3.14
174	3.45 ± 0.16	2.06 ± 0.10	1.67 ± 0.07	3.12
Average	–	–	1.65 ± 0.09	3.17

All data variances computed at the 99% Student t level.

Table 6
Comparative KDIE values for exothermic liquid state DNNC and RDX thermochemical decomposition process

Temperature range (°C)	Reference	Compound	Analysis method	KDIE value
174–194	This work	DNNC/DNNC-d_6	Isothermal DSC	1.65
227–242	11	RDX/RDX-d_6	Isothermal DSC	1.64
212 only	11	RDX/RDX-d_6	Isothermal QUVA[a]	1.57
206–216	12	RDX/RDX-d_6	Isothermal TGA	1.56

[a] Quenched Ultra-Violet Absorbance measurement.

For comparison, molecular KDIE-based IDSC analyses of the solid state DNNC thermochemical decomposition process also reveal a primary 1.47 KDIE and a rate-controlling C–H bond rupture for the exothermic acceleratory portion of the decomposition process. In contrast to the liquid DNNC decomposition results, however, the solid state DNNC induction period affords a secondary 1.22 KDIE value suggesting that homolytic ring C–N ring bond cleavage likely constitutes the endothermic rate-controlling feature prior to transitioning into the exothermic acceleratory phase [2].

The homolytic rate-controlling chemical bond rupture, and resultant atom transfer during the decomposition process of an energetic compound, depends upon its chemical structure and resultant chemical environment [23]. As seen in Fig. 9, the TNT molecule possesses a chemical structure where two types of C–H bonds reside in vastly different chemical environments. This is reflected by the large proton NMR shifts between the C–H bonds of the saturated aliphatic pendant methyl ($-CH_3$) group and the aromatic phenyl C–H bonds ($\Delta = 6.32$ ppm). TNT forms mainly condensed phase products during thermochemical decomposition [41,42] via a rate-controlling C–H bond rupture at the pendant methyl group site [10], and the aromatic C–H bonds remain intact when forming these condensed phase decomposition products [9,10,41,42]. The chemical structure of the DNNC, where all C–H bonds are embodied in saturated aliphatic ring methylene groups, represents a far different structural environment from TNT (Fig. 9).

The rate-controlling C–H bond rupture found in the exothermic liquid state DNNC thermochemical decomposition process only can emanate from the saturated methylene groups in the DNNC ring structure (Fig. 2), but the differences in their chemical environment are much more subtle than with TNT. This subtle difference in DNNC molecular structure, and resultant chemical environment, is illustrated by the very small NMR proton shift between the two C-2 methylene protons versus the four C-4/C-6 methylene protons ($\Delta = 0.83$ ppm) seen in Fig. 9. While the two methylene groups at the C-4 and C-6 DNNC ring positions are chemically and structurally equivalent, the methylene at the C-2 position is neither chemically nor structurally equivalent with the C-4 and C-6 methylenes. This subtle difference in the DNNC chemical structure raises two questions. Are all three methylene groups in the DNNC ring structure the source for this rate-controlling C–H bond rupture for the DNNC thermochemical decomposition process, like that found in RDX with its three equivalent methylenes? Or, secondly, is the structural and resultant chemical non-equivalence of the DNNC ring

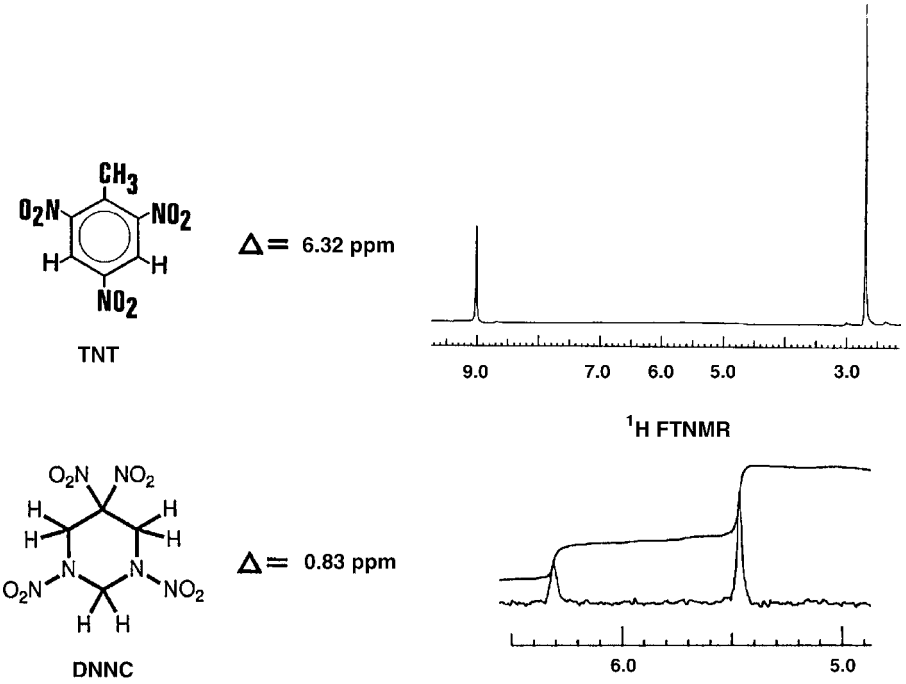

Fig. 9. Comparative proton NMR chemical shift magnitudes of TNT C–H bonding ($\Delta = 6.32$ ppm) versus DNNC ring methylene C–H bonding ($\Delta = 0.83$ ppm).

structure sufficiently different to restrict this C–H bond rupture to either the equivalent C-4/C-6 methylene sites, or alternatively, to the non-equivalent nitrogen sandwiched C-2 site? An investigative mechanistic IDSC comparison of the four DNNC, DNNC-d_2, DNNC-d_4, and DNNC-d_6 isotopomers enters into the DNNC molecule and differentiates between these chemically similar DNNC ring methylenes. In doing so, it determines the structural site from which C–H bond rupture ultimately regulates the DNNC thermochemical decomposition process. A similar approach was used for the nitroraromatic HNS (hexanitrostilbene) compound to analyze the more chemically diverse aromatic and vinyl C–H bonds contained in its molecular structure, but no primary KDIE or resultant rate-controlling C–H bond rupture was found [43].

3.3. Structural kinetic deuterium isotope effect

A structural KDIE represents an approach which compares different internal structural features of a given compound by using both the unlabeled compound (DNNC) and the perdeuterio-labeled compound (DNNC-d_6), as bracketed baseline data, against analogous, partially labeled isotopomers (DNNC-d_2, DNNC-d_4). There is a 9.6 kJ/mol energy difference between the C–H bond ground state vibrational energy and that of the analogous but stronger C–D bond. If bond energy differences between the non-equivalent C-2 methylene and the equivalent C-4/C-6 methylene positions in the unsymmetrical DNNC molecule are greater than 9.6 kJ/mol, selectively deuterium-labeled DNNC-d_2 and DNNC-d_4 isotopomers could reveal which methylene position provides the rate-controlling C–H bond rupture for the DNNC decomposition process. Consistent with the KDIE concept, if the DNNC-d_2 and DNNC-d_4 isotopomers seen in Fig. 10 were synthesized and subjected to IDSC analyses, the methylene position providing the rate-controlling C–H bond rupture could be identified. Should the C-2 methylene position exclusively provide this rate-controlling C–H bond rupture, then the partially labeled DNNC-d_2 isotopic isomer would give the same slower rate constant (k_{d2}) as DNNC-d_6 (k_{d6}), and the partially deuterium-labeled DNNC-d_4 would give the same rate constant (k_{d4}) as DNNC (k). Conversely, if the chemically equivalent C-4/C-6 methylenes are the source of the C–H rate-controlling bond cleavage, DNNC-d_2 would have the same rate constant (k_{d2}) as DNNC (k), and DNNC-d_4 (k_{d4}) should give the same rate constant as does the slower one exhibited by DNNC-d_6 (k_{d6}).

The partially labeled isotopic isomers, DNNC-d_2 and DNNC-d_4, were synthesized (Section 2) where discreet perdeuterio –CD_2– methylene groups are introduced into the DNNC molecular structure. To the nearest whole number, proton NMR integration verified that each contained the intended two and four deuterium atoms, respectively. However, for both the synthesized DNNC-d_2 and DNNC-d_4 compounds, proton NMR integration for the specific C-2 and C4/C-6 methylenes showed a 1:2 integration ratio indicating that random –CD_2– methylene scrambling into all three DNNC ring positions resulted with both isotopomers. Under the alkaline reaction conditions, it was found that all three C-2, C-4, and C-6 positions in the DNNC ring structure are subject to a formylation/deformylation equilibrium involving intermixing formaldehyde molecules which are generated from the ADIOL reactant and available from the additional formaldehyde reactant. Unfortunately, this equilibrium exchange occurred faster than did ring self-assembly (Fig. 11).

Mass spectral analysis of the synthesized DNNC-d_2 and DNNC-d_4 samples revealed that each contained a mixture of all four isotopomers, DNNC, DNNC-d_2, DNNC-d_4, and DNNC-d_6, in percentages that mirrored the intended pure, selectively

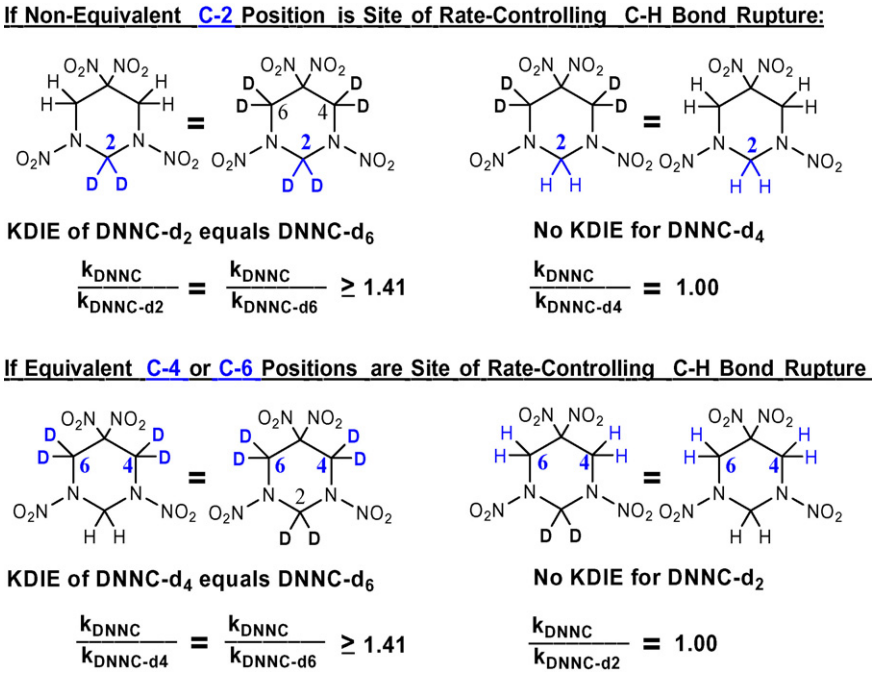

Fig. 10. Theoretical KDIE results with specific partially deuterium-labeled DNNC-d_2 and DNNC-d_4 isotopomers.

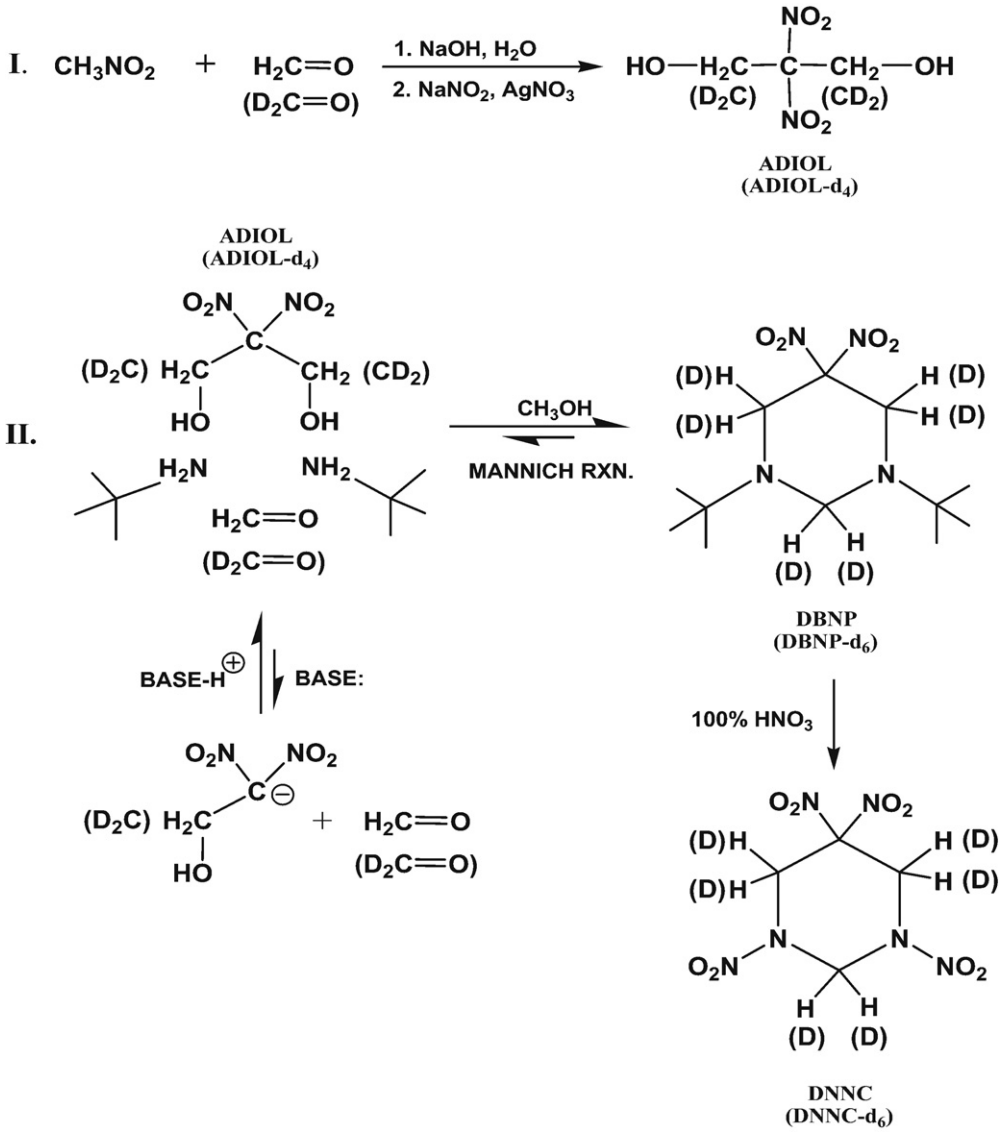

Fig. 11. General synthesis scheme used for ADIOL, ADIOL-d_4 and the four DNNC isotopomers.

positioned isotopic isomers DNNC-d_2 and DNNC-d_4 seen in Fig. 10. The DNNC-d_2 isotopomer predominated in the mixed, synthesized DNNC-d_2 sample, and the DNNC-d_4 isotopomer was predominant in the mixed, synthesized DNNC-d_4 sample. The net result of this random $-CD_2-$ methylene ring incorporation, and the resultant percent mixtures of all four isotopic isomers in the synthesized DNNC-d_2 and DNNC-d_4 samples, produced bulk materials where the DNNC-d_2 behaved as if it were one-third deuterium atom labeled at each methylene (C-2, C-4, and C-6) ring position, and the DNNC-d_4 bulk material behaved as if it were two-thirds deuterium labeled at each methylene position (Fig. 12). This serendipitous result necessitated using a modified and slightly more complex approach to determine whether or not a specific methylene group in the DNNC chemical structure is responsible for the rate-controlling C–H bond rupture.

Initially, it was surmised that such random isotopic methylene group scrambling possibly explained the partial rate reductions seen as one progresses from DNNC to DNNC-d_2, DNNC-d_4, and finally to DNNC-d_6 (Table 7) without revealing any mechanistic differentiation between the two dissimilar DNNC methylene groups [44]. An evolving mechanistic analysis, however, suggested otherwise.

Random isotopic methylene scrambling could only give this result if the DNNC molecule predominantly decomposes with the ring structure immediately unraveling to form one neutral $CH_2{=}CNO_2)_2$, and two $CH_2{=}NNO_2$ fragments, or even lower molecular weight species, prior to any rate-controlling C–H bond rupture occurring. If this were the case, a molecular KDIE reflecting a secondary value should have been observed. Observation of a primary KDIE value strongly suggests this is not the case and that the skeletal ring structure primarily stays intact through the initial and subsequent rate-controlling C–H bond rupture.

Secondly, past condensed phase product isolation studies with TNT [41,42] and TATB [19] show intact ring structures where decomposition reactions occur only with the pendant methyl, amino, and nitro groups and include those consis-

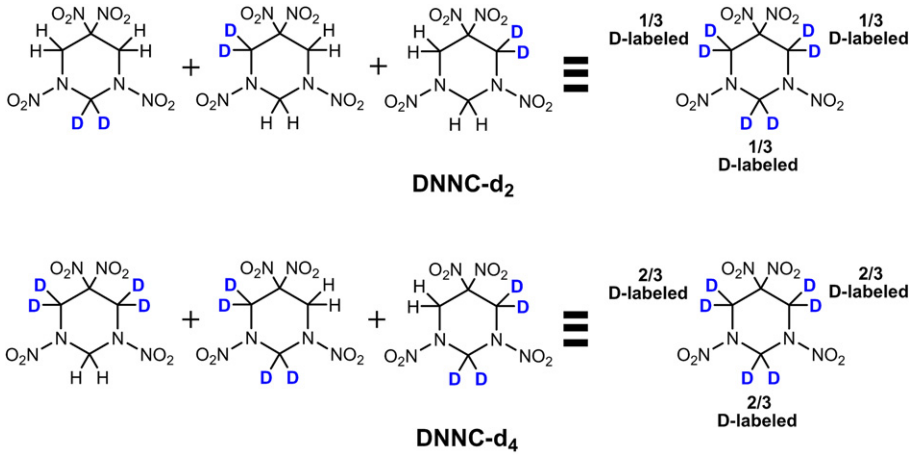

Fig. 12. Overall kinetic behavior of random partially deuterium-labeled DNNC-d_2 and DNNC-d_4 isotopomer bulk samples.

tent with the KDIE-determined rate-controlling C–H (TNT) [10] and N–H (TATB) [3] bond ruptures. Ring structures are left intact, and initial reactions with nitramines appear to involve the pendant NO_2 group [5,8] and subsequent rate-controlling ring hydrogen atom rupture by NO_2 radical abstraction [8].

Thirdly, sub-initiation impact and shock studies, where the charred inner surfaces of hot spots caused by a rapid thermochemical decomposition process, also reveal condensed phase intermediate condensed phase products with intact ring structures for TNT [22], TATB [21], and RDX [14,20]. In the case of structurally related RDX, sub-initiation by impact displays trigger linkage or first reaction N–O bond rupture to form the analogous trinitroso intermediate compound [45]. More drastic sub-initiated shock reveals a melamine type of product where C–H bond rupture [20], the rate-controlling step reflected by KDIE-based thermochemical decomposition investigations [11,12], apparently follows the initial N–O bond rupture, and again, leaves the skeletal ring structure intact as discussed in Section 1.

A primary molecular KDIE, involving a rate-controlling C–H bond rupture, occurs early during the condensed phase thermochemical decomposition process and involves an intermediate DNNC radical with an intact skeletal ring structure. Literature precedence also suggests that the skeletal ring structure of cyclic energetic materials is attacked late during the thermochemical decomposition process after the rate-controlling bond rupture occurs [2,3,5,8–10,12,24,25,28,29,41,42,45,46]. Therefore, the consistent decrease in DNNC decomposition rate with increased deuterium substitution in Table 7 cannot be a random occurrence under these documented mechanistic circumstances. A more complex modified evaluative approach is required for mechanistic consistency [30].

This modified approach invokes two reasonable assumptions. First, when possible, the homolytic, covalent C–H bond rupture, and H atom transfer, will always occur in preference to that of the stronger C–D covalent bond. Secondly, should the rate-controlling step involve and be forced to proceed at one specific DNNC methylene site, and this methylene site is deuterium labeled, then C–D bond rupture will occur with a concomitant decrease in the decomposition rate and associated rate constant.

Fig. 12 represents a valid model with which to evaluate kinetics data obtained with DNNC and its three deuterium-labeled isotopomers, DNNC-d_2, DNNC-d_4, and DNNC-d_6. Fig. 12 (top)

Table 7
IDSC rate constant data reduction for the DNNC and its deuterated isotopomers

Kinetic data	DNNC	DNNC-d_2	DNNC-d_4	DNNC-d_6
Rate constant (k in s^{-1})	7.79×10^{-3} ± 0.25	6.84×10^{-3} ± 0.30	5.92×10^{-3} ± 0.57	**4.68×10^{-3}** ± 0.61
Interval (s^{-1})		0.95×10^{-3}	0.92×10^{-3}	**1.24×10^{-3}**
Percent k reduction	0%	31%	60%	100%
Accel. phase linearity (%)	93	89	88	76
No. runs	6	5	5	5

All data variances computed at the 99% Student *t* level.

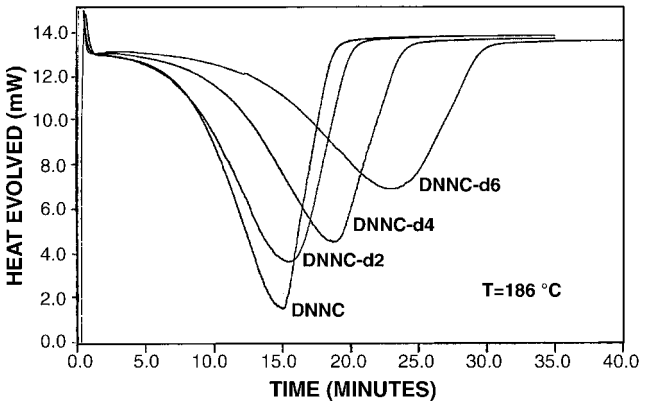

Fig. 13. Comparison of individual DNNC, DNNC-d_2, DNNC-d_4, and DNNC-d_6 isotopomer thermograms at 186 °C.

displays three –CD_2– randomly labeled DNNC-d_2 molecules, which combined, mirror the synthesized DNNC-d_2 isotopic isomer that behaves as if it were one-third deuterium labeled at each methylene position. If the rate-controlling C–H bond rupture emanates from the C-2 methylene site, slower C–D bond cleavage would occur only one out of three times, and C–H bond rupture would occur twice as often. Thus, DNNC-d_2 should give a one third (33%) rate constant reduction between the faster unlabeled DNNC rate constant and the relative 100% rate constant reduction of DNNC-d_6. Alternatively, if the equivalent C-4/C-6 methylene positions are the source for the rate-controlling C–H bond rupture, a slower C–D bond rupture, and concomitant rate constant reduction would not occur with the DNNC-d_2 isotopic isomer because a preferred C–H bond rupture is always available. Fig. 12 (bottom) displays three –CD_2– randomly labeled DNNC-d_4 molecules, which combined, mirror the synthesized DNNC-d_4 isotopic isomer that behaves as if it were two-thirds deuterium labeled at each methylene position. With the synthesized DNNC-d_4 isotopic isomer, a C–H rate-controlling bond rupture relegated to the C-2 methylene would effect a two-thirds (67%) rate constant reduction since this methylene site is deuterated two out of three times. If the rate-controlling step were provided by the C-4/C-6 sites, DNNC-d_4 would give a one third (33%) rate constant reduction. This is summarized in Table 8.

The DNNC, DNNC-d_2, DNNC-d_4, and DNNC-d_6 thermochemical decomposition processes were analyzed by IDSC at 186 °C, and a systematic rate reduction was observed. Fig. 13 shows an individual IDSC run for each isotopic isomer where the decomposition rate progressively slows in the order: (fastest) DNNC > DNNC-d_2 > DNNC-d_4 > DNNC-d_6 (slowest). The fact that, both the DNNC-d_2 and DNNC-d_4 rate constants are reduced significantly (Table 8) during the exothermic accelerator phase, immediately identifies the C-2 methylene position as being the structural site for the rate-controlling C–H bond rupture for this portion of the thermochemical decomposition process.

Table 8
Expected rate constant reduction of methylene sites relative to DNNC/DNNC-d_6 rate constant difference

Isotopomer compound	RCS at C-2 rate constant reduction (%)	RCS at C-4/C-6 rate constant reduction (%)
DNNC-d_2	33	0
DNNC-d_4	67	33
DNNC-d_6	100	100

RCS = rate-controlling step (C–H bond rupture).

Careful rate constant data analysis of the experimental structural KDIE data in Table 8 shows that, within the total rate difference between DNNC and fully deuterium-labeled DNNC-d_6, DNNC-d_2 decomposes about one-third (31%) more slowly than DNNC, and DNNC-d_4 nearly two-thirds (60%) more slowly (Table 8). That is, the structural KDIE rate reduction percent for DNNC-d_2 equals [k_{DNNC}–$k_{DNNC\text{-}d_2}$ divided by k_{DNNC}–$k_{DNNC\text{-}d_6}$] (from Table 7) times 100, and the structural KDIE rate reduction percent for DNNC-d_4 equals [k_{DNNC}–$k_{DNNC\text{-}d_4}$ divided by k_{DNNC}–$k_{DNNC\text{-}d_6}$] times 100. This data very closely matches the calculated criteria expected if the non-equivalent C-2 methylene position in the DNNC molecule is the origin for the rate-controlling C–H bond rupture site, and further experimental data analysis strengthens this conclusion.

Rate constant interval differences in Table 8 reveal nearly identical interval reductions between the DNNC and DNNC-d_2 rate constant values, and between the DNNC-d_2 and DNNC-d_4 rate constants; however, a much larger $1.24 \times 10^{-3}\ s^{-1}$ interval reduction appears between the DNNC-d_4 and DNNC-d_6 rate constants. Fig. 14 displays this data in graph plot form and further suggests the experimental DNNC-d_6 rate constant, while quite reasonable, might actually be slightly lower than what is consistent with the other DNNC, DNNC-d_2, and DNNC-d_4 isotopomers. Plotting the number of hydrogen atoms (x-axis) in each DNNC isotopomer [47], versus the measured rate constant (y-axis) in Fig. 14, affords an excellent linear least squares fit ($R^2 = 0.994$), but Fig. 14 also gives a linear-intercept value for DNNC-d_6 (0 H-atoms) [47] which suggests a rate constant equal to $4.77 \times 10^{-3}\ s^{-1}$, rather than the lower $4.68 \times 10^{-3}\ s^{-1}$, would be more reasonable [48].

By graphing only the first three points corresponding to DNNC, DNNC-d_2, and DNNC-d_4 in an analogous plot (Fig. 15), a near perfect linear least squares fit ($R^2 = 0.9999$ or 1.000) results and gives a y-intercept value at the DNNC-d_6 (0 H-atoms)

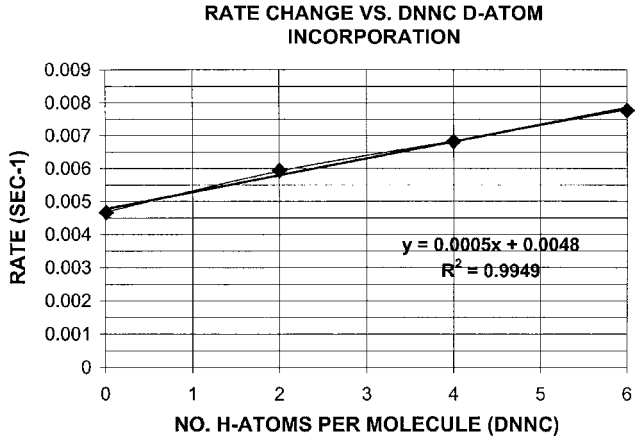

Fig. 14. Experimental DNNC isotopomer rate constant versus number of methylene hydrogen atoms in DNNC molecular structure.

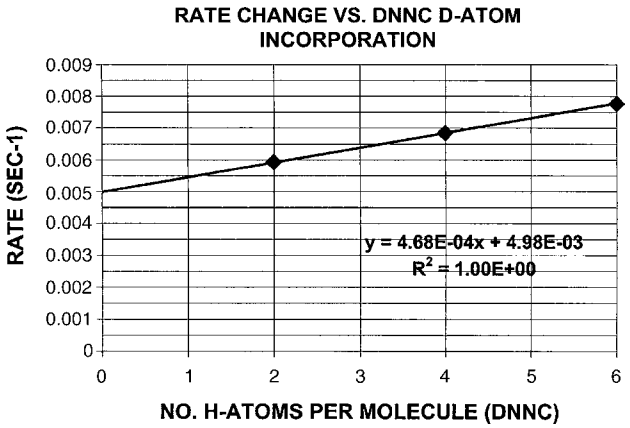

Fig. 15. Experimental DNNC isotopomer rate constant versus number of methylene hydrogen atoms in DNNC molecular structure with DNNC-d_6 (H = 0 atoms) isotopomer rate constant not plotted.

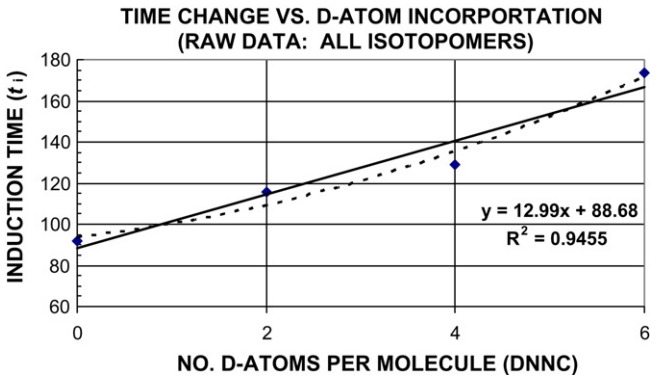

Fig. 16. Experimental DNNC isotopomer induction period times from Table 10 versus number of methylene deuterium atoms in DNNC molecular structure.

isotopomer that defines a $4.98 \times 10^{-3}\ s^{-1}$ revised rate constant value. When this revised rate constant ($4.98 \times 10^{-3}\ s^{-1}$) is substituted for the $4.68 \times 10^{-3}\ s^{-1}$ experimental data rate constant in Table 9, all three rate constant reduction interval differences match much more closely with the re-computed DNNC-d_4 to DNNC-d_6 interval falling between the two other intervals. Most importantly, a 34% rate constant reduction, versus calculated 33%, results for DNNC-d_2, and the expected 67% rate reduction surfaces for DNNC-d_4. Thus, the rate-controlling C–H bond rupture, which regulates the energy release rate of the exothermic acceleratory phase, originates at the non-equivalent C-2 methylene site sandwiched between the two DNNC ring nitrogen atoms.

Next, the induction period data is similarly evaluated to determine if this mechanistic feature also regulates this earlier portion of the DNNC thermochemical decomposition process. Induction period times also represent rate measurement data and have an inversely proportional relationship with corresponding reaction rate constants which cannot be directly measured by IDSC in this flat portion of the thermogram [10]. A fast endothermic reaction rate (large rate constant), occurring during the induction period, provides a short (small) induction time. Therefore, induction times should increase as the amount of deuterium-labeled methylene groups increase in the DNNC isotopomer by the proportionate percentages shown in parentheses: DNNC (0% baseline time) < DNNC-d_2 (33%) < DNNC-d_4 (67%) < DNNC-d_6 (100% maximum time).

Table 10 lists the averaged induction time (t_i) obtained at 186 °C for DNNC and each of its three deuterium labeled isotopomers. The increased induction times for both DNNC-d_2 and DNNC-d_4, compared to DNNC (Fig. 16), again suggests that the rate-controlling C–H bond rupture emanates from the C-2 methylene site of the DNNC ring structure. Should this rate-controlling mechanistic feature be generated from the equivalent C-4 and C-6 methylenes, no induction time decrease for the DNNC-d_2 isotopomer, compared to DNNC, should result (Fig. 12). Induction time interval differences between DNNC/DNNC-d_2, DNNC-d_2/DNNC-d_4, and DNNC-d_4/DNNC-d_6 do not follow the expected regular magnitude increase which should give a 33% induction time increase for

Table 9
Revised DNNC-d_6 rate constant data for DNNC and its deuterated isotopomers at 186 °C

Kinetic data	DNNC		DNNC-d_2		DNNC-d_4		DNNC-d_6
Rate constant (k in s^{-1})	7.79×10^{-3}		6.84×10^{-3}		5.92×10^{-3}		**4.98×10^{-3}**
Interval (s^{-1})		0.95×10^{-3}		0.92×10^{-3}		**0.94×10^{-3}**	
Percent k reduction	0%		34%		67%		100%

Table 10
Induction time data for DNNC and its partially deuterated isotopomers at 186 °C

Induction period data	DNNC	Interval	DNNC-d_2	Interval	DNNC-d_4	Interval	DNNC-d_6
No. IDSC runs	6		5		5		5
Ave. induction time (s)	91.8 ± 23.0		115.7 ± 13.8		**129.2** ± 25.1		173.9 ± 34.1
Interval (s)		23.9		**13.5**		**44.7**	
Percent reduction (%)	0		29		**46**		100

All data variances computed at the 99% Student t level.

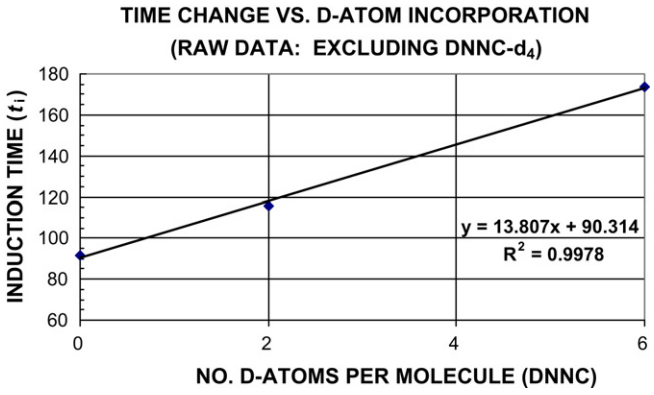

Fig. 17. Experimental DNNC isotopomer induction period time versus number of methylene deuterium atoms in DNNC molecular structure with DNNC-d_4 isotopomer induction time not plotted.

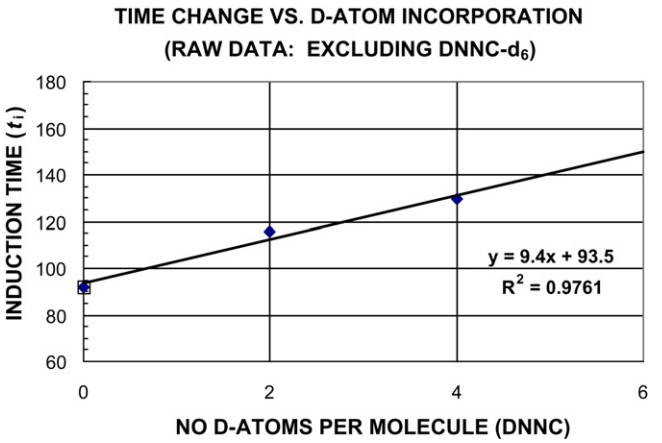

Fig. 18. Experimental DNNC isotopomer induction period time versus number of methylene deuterium atoms in DNNC molecular structure with DNNC-d_6 isotopomer induction time not plotted.

DNNC-d_2 and a 67% increase for DNNC-d_4. Rather, induction time increases are 29 % for DNNC-d_2 and 46% for DNNC-d_4 using the initial experimental interval data obtained (Table 10).

Again, like the exothermic acceleratory phase data, an extended treatment of the induction time data clearly reflects the expected trend. A graphic trend line plot of experimental induction times versus the number of hydrogen atoms in DNNC, DNNC-d_2, DNNC-d_4, and DNNC-d_6 (Table 10), only gives an $R^2 = 0.946$ linear least squares fit (Fig. 16); but, comparison of a polynomial curved trend line and close examination of the linear trend line and interval differences from Table 10, suggest the induction time for DNNC-d_4 may be low compared to the other three isotopomers.

In contrast to Fig. 16, Fig. 17 plots a least squares trend line fit for the induction times of DNNC, DNNC-d_2, and DNNC-d_6 only, where the DNNC-d_4 129.2 s induction time data is excluded, and affords an excellent $R^2 = 0.998$ linear fit with a 13.81 slope value. A similar plot that includes the DNNC, DNNC-d_2, and DNNC-d_4 induction times, but excludes the DNNC-d_6 173.9 s induction time (Fig. 18), gives a much lower $R^2 = 0.976$ fit, and verifies that the abnormally low induction time comes from DNNC-d_4 rather than DNNC-d_6.

Averaging the sum of the three induction time interval values found in Table 10, an interval of 27.4 s results over the entire DNNC to DNNC-d_6 isotopomer range. Substituting this averaged 27.4 s interval difference for the questionable 13.5 s interval difference between DNNC-d_2 and DNNC-d_4, and adding the 27.4 s to the 115.7 s induction time of DNNC-d_2, a 143.1 s induction time for DNNC-d_4 results which nearly matches the upper 99% Student t variance for this questionable 129.2 s induction period value. The calculated 27.4 s induction time interval,

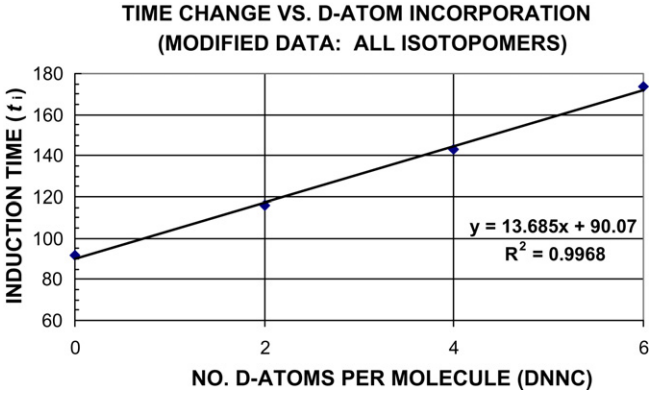

Fig. 19. Experimental DNNC isotopomer induction period times versus number of methylene deuterium atoms in DNNC molecular structure with DNNC-d_4 isotopomer modified induction time plotted from Table 11.

and resultant calculated 143.1 s induction time for DNNC-d_4, along with a revised 30.8 s interval difference in place of 44.7 s between DNNC-d_4 and DNNC-d_6 to maintain a 173.9 s induction time for DNNC-d_6, are substituted for the corresponding data in Table 10 to give Table 11. Using the revised data from Table 11, the DNNC-d_2 induction time increase remains at 29% for DNNC-d_2, but becomes a much more reasonable 62% for DNNC-d_4. The 29% DNNC-d_2 induction time increase is reasonably close to the expected 33% value, and the corrected 62% induction time increase for DNNC-d_4 (Table 11), versus 46% from Table 10, compares more favorably with the calculated 67% induction time increase expected.

Table 11
Revised induction time data for DNNC and its partially deuterated isotopic isomers

Induction period data	DNNC	Interval	DNNC-d_2	Interval	DNNC-d_4	Interval	DNNC-d_6
No. IDSC Runs	6		5		5		5
Ave. induction time (s)	91.8		115.7		**143.1**		173.9
Interval (s)		23.9		**27.4**		**30.8**	
Percent reduction (%)	0		29		**62**		100

A graphic plot of the revised induction time data in Table 11 for DNNC, DNNC-d_2, DNNC-d_4, and DNNC-d_6 generates a linear trend line with a nearly identical linear $R^2 = 0.997$ fit and 13.68 slope (Fig. 19) as that seen with the linear $R^2 = 0.998$ value and 13.81 slope found in Fig. 16 where the suspect DNNC-d_4 induction time is excluded. Allowing that visually interpreted induction time data measurements are not as exact as accelerator phase rate constants, this induction time data treatment further confirms that C–H bond rupture at the DNNC structural C-2 methylene position also controls the endothermic induction period portion of the liquid state DNNC thermochemical decomposition process.

4. Conclusions

Liquid state thermochemical decomposition of DNNC, conducted between 174 and 194 °C, is an autocatalytic process. During this process homolytic covalent C–H bond rupture, and resultant hydrogen atom transfer, constitute a key mechanistic feature which determines the endothermic initiation and subsequent exothermic propagating energy release rates.

Molecular KDIE data, taken with unlabeled DNNC and perdeuterio-labeled DNNC-d_6, displays a primary KDIE value for both the endothermic induction period and subsequent autocatalytic exothermic acceleratory phase (Fig. 20, top). The initial endothermic induction period likely generates a catalytic species via a rate-controlling homolytic C–H bond rupture (KDIE = 1.76), which upon reaching a threshold concentration, initiates an exothermic autocatalytic decomposition process. The exothermic decomposition process then follows a rate that also is controlled by a homolytic C–H bond rupture (KDIE = 1.65) coming from one of the methylene groups comprising the DNNC ring structure. A significantly higher energy of activation is required to initiate the DNNC endothermic induction period (170.0 kJ/mol) than what is needed for the corresponding exothermic acceleratory portion of the respective decomposition process (104.2 kJ/mol). The 65.8 kJ/mol energy difference, coupled with its autocatalytic rate behavior supports this catalytic mechanistic interpretation for the liquid state DNNC thermochemical decomposition process. This same mechanistic trend previously was reported for the solid state DNNC thermochemical decomposition process (Table 3) [2].

Structural KDIE data, obtained from comparing DNNC and perdeuterio-labeled DNNC-d_6 with partially deuterium-labeled isotopomers DNNC-d_2 and DNNC-d_4, enters into the DNNC molecular ring structure and reveals that the rate-controlling C–H bond rupture originates at the methylene (–CH_2–) site at the C-2 position of the DNNC molecule which is sandwiched between the two ring nitrogen atoms, or originates from a structural fragment that is generated from this structural site (Fig. 20, bottom). The chemically and structurally equivalent methylene groups at the C-4 and C-6 positions of the DNNC molecule reside in a chemical environment which is subtly different from the third C-2 methylene group. The subtle energy difference of the chemical environments between the C-2 methylene site and the C-4/C-6 equivalent methylene sites, or the corresponding structural fragments that provide the rate-controlling C–H bond rupture, must exceed the 9.6 kJ/mol ground state vibrational energy difference between the C–H and C–D bond. If this were not the case, the rate-controlling C–H bond rupture, and hydrogen atom transfer, would occur randomly at all three DNNC methylene positions. The C-4/C-6 methylenes contribute little or no significant role in determining the overall liquid state DNNC thermochemical decomposition and energy release rates.

Apparently, the liquid state DNNC induction period requires a higher activation energy (170 kJ/mol) than does the solid state (128 kJ/mol) [2] to initiate the subsequent exothermic portion of the thermochemical decomposition process. The liquid state (104 kJ/mol) and solid state (105 kJ/mol) [2] DNNC exothermic acceleratory phases have a similar activation energy once energy release commences. While homolytic C–H bond rupture determines both the endothermic induction time duration and the exothermic acceleratory phase energy release rate in liquid state DNNC thermochemical decomposition, rate-controlling homolytic C–H bond dissociation only is found during the acceleratory phase of the solid state thermochemical decomposition process. Solid state DNNC endothermic induction period kinetics appear to be regulated by a different rate-controlling bond rupture as previously reported [2].

Acknowledgements

We gratefully acknowledge the Air Force Office of Scientific Research (AFOSR) for funding this research study. The authors thank Dr. John L. Belletire (ERC, Inc. @ AFRL Edwards) for several thorough manuscript reviews and productive technical discussions, and AFRL colleagues, Mr. Joel W. Beckmann, and Dr. Robert C. Corley for technical processing support, Dr. Jeffrey

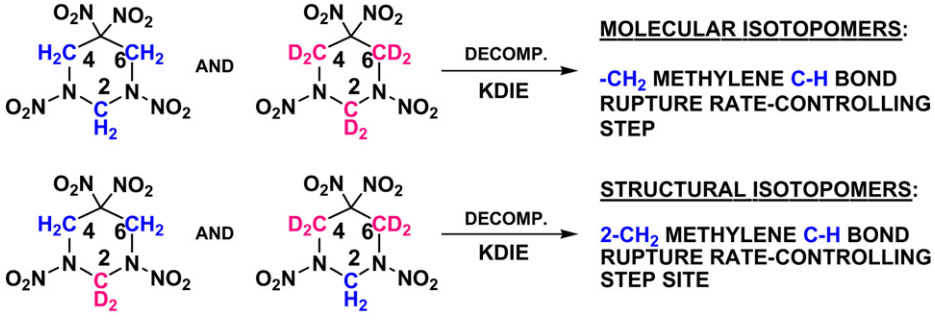

Fig. 20. Graphic conclusion for liquid state DNNC thermochemical decomposition findings.

D. Mills (AFRL) for delineating a key technical point, Dr. Tae-Woo Park for statistical assistance, Dr. Stephen D. Champbreau, and Dr. Jerry A. Boatz for salient kinetics discussion. Dr. Ronald E. Channell (dec. 25 Feb 2007) and Mr. Wayne M. Kalliomaa provided AFRL managerial and administrative support, and Mr. Dean Richards (AFRL) contributed critical computer graphics support. Dr. Gary S. Buckley (Cameron University, Lawton, OK) accomplished and shared early IDSC software data transfer insights. Dr. Kenneth A. Martin, Dr. Victor E. Heasley, and Dr. Dale F. Shellhamer, Department of Chemistry, Pt. Loma Nazarene University, San Diego, CA contributed helpful scientific discussions, initial software support, and key initial on-site computer assistance.

References

[1] A.K. Galwey, M.E. Brown, Thermal Decomposition of Ionic Solids, Elsevier, Amsterdam, The Netherlands, 1999, pp. 1–2.
[2] S.A. Hendrickson, S.A. Shackelford, Thermochim. Acta 440 (2006) 146–155, and references therein.
[3] R.N. Rogers, J.L. Janney, M.H. Ebinger, Thermochem. Acta 59 (1982) 287–298.
[4] T.B. Brill, D.G. Patil, J. Duterque, G. Lengelle, Combust. Flame 95 (1993) 183–190.
[5] Y. Shu, B.L. Korsounskii, G.M. Nazin, Russ. Chem. Rev. 73 (2004) 293–307.
[6] S. Zeman, Propell. Explos. Pyrotech. 25 (2000) 66–74.
[7] S. Zeman, Propell. Explos. Pyrotech. 28 (2003) 308–313, and references therein.
[8] S.A. Shackelford, M.B. Coolidge, B.B. Goshgarian, B.A. Loving, R.N. Rogers, J.L. Janney, M.H. Ebinger, J. Phys. Chem. 89 (1985) 3118–3126, and references therein.
[9] S.A. Shackelford, in: S.N. Bulusu (Ed.), Chemistry and Physics of Energetic Materials, NATO Advanced Study Institute Series, Series C, vol. 309, Kluwer Academic Publishers, Dordrecht, NL, 1990, pp. 413–432, and references therein (Chapter 18).
[10] S.A. Shackelford, J.W. Beckmann, J.S. Wilkes, J. Org. Chem. 42 (1977) 4201–4206.
[11] S.L. Rodgers, M.B. Coolidge, W.J. Lauderdale, S.A. Shackelford, Thermochim. Acta 177 (1991) 151–168.
[12] S.N. Bulusu, D.J. Weinstein, J.R. Autera, R.W. Velicky, J. Phys. Chem. 90 (1986) 4121–4126.
[13] S.A. Shackelford, 10th New Trends in Research of Energetic Materials: Performance and Decomposition, Pardubice, CZ, April 25–27, 2007.
[14] S.A. Shackelford, in: S.N. Bulusu (Ed.), Chemistry and Physics of Energetic Materials, NATO Advanced Study Institute Series C, vol. 309, Kluwer Academic Publishers, Dordrecht, NL, 1990, pp. 433–456, and references therein (Chapter 19).
[15] S.A. Shackelford, B.B. Goshgarian, R.D. Chapman, R.E. Askins, D.A. Flanigan, R.N. Rogers, Propell. Explos. Pyrotech. 14 (1989) 93–102.
[16] S.A. Shackelford, S.L. Rodgers, R.E. Askins, Propell. Explos. Pyrotech. 16 (1991) 279–286.
[17] S.N. Bulusu, J.R. Autera, J. Energetic Mater. 1 (1983) 133–140.
[18] J. Sharma, W.L. Garrett, F.J. Owens, V.L. Vogel, J. Phys. Chem. 86 (1982) 1657–1661.
[19] J. Sharma, J.C. Hoffsommer, D.J. Glover, C.S. Coffey, F. Santiago, A. Stolovy, S. Yasuda, in: J.R. Asay, R.A. Graham, G.K. Straub (Eds.), Shock Waves in Condensed Matter-1983, Elsevier Science Publishers, Amsterdam, NL, 1984, pp. 543–546.
[20] J. Sharma, J.C. Hoffsommer, D.J. Glover, C.S. Coffey, J.W. Forbes, T.P. Liddiard, W.L. Elban, F Santiago, Eighth International Symposium on Detonation, Albuquerque, NM, July 15–19, 1985, pp. 725–733.
[21] J. Sharma, J.W. Forbes, C.S. Coffey, T.P. Liddiard, J. Phys. Chem. 91 (1987) 5139–5144.
[22] J. Sharma, J.W. Forbes, C.S. Coffey, T.P. Liddiard, in: S.C. Schmidt, N.C. Holmes (Eds.), Shock Waves in Condensed Matter-1987, Elsevier Science Publishers, Amsterdam, NL, 1988, pp. 565–568.
[23] S.A. Shackelford, J. de Phys. IV (Colloque C4) 5 (1995) C4-485–C4-499.
[24] R.A. Fifer, in: K.K. Kuo, M. Summerfield (Eds.), Progress in Astronautics and Aeronautics, vol. 90, AIAA Inc., New York, 1984, pp. 177–237.
[25] R. Behrens Jr., S. Bulusu, J. Phys. Chem. 96 (1992) 8877–8891.
[26] R. Behrens Jr., S. Bulusu, J. Phys. Chem. 94 (1990) 6706–6718.
[27] R. Behrens Jr., S. Bulusu, J. Phys. Chem. 95 (1991) 5838–5845.
[28] R. Behrens Jr., S. Bulusu, J. Phys. Chem. 96 (1992) 8891–8897.
[29] S. Maharrey, R. Behrens Jr., J. Phys. Chem. 109 (2005) 11236–11249.
[30] S.A. Shackelford, J.G. Goldman, J.A. Menapace, S.A. Hendrickson, 35th International Annual Conference of ICT: Energetic Materials Structure and Properties, DWS Werbeagentur und Verlag GmbH, Karlsruhe, Germany, June 29–July 2, 2004, pp. 43-1–43-15.
[31] S.A. Shackelford, J.F. Goldman, Propell. Explos. Pyrotech. 20 (1995) 1–4, and references therein.
[32] R.N. Rogers, RCEM Rpt. A-04-87, Research Center for Energetic Materials, New Mexico Tech., Socorro, NM 87081, USA, November 4, 1987, pp. 15–65.
[33] S.A. Shackelford, J. Labeled Compd. Radiopharm. XXIX (1991) 1197–1206.
[34] D.L. Levins, C.D. Bedford, C.L. Coon, U.S. Patent 4,346,222 (1982) (SRI International, USA).
[35] D.A. Cichra, H.G. Adolph, J. Org. Chem. 47 (1982) 2472–2476.
[36] J. Boileau, M. Piteau, G. Jacob, Propell. Explos. Pyrotech. 15 (1990) 38 (the subject DNNC compound also has appeared in the literature under the acronym of TNDA).
[37] H.H. Cady, R.N. Rogers, Los Alamos Tech. Rpt. 2696, Los Alamos Laboratory, Los Alamos, NM, April 1962.
[38] B.D. Roos, T.B. Brill, Propell. Explos. Pyrothech. 28 (2003) 65–71.
[39] T.H. Lowry, K.S. Richardson, Mechanism and Theory in Organic Chemistry, second ed., Harper and Row, New York, 1981, pp. 206–207.
[40] G.W. Klump, Reactivity in Organic Chemistry, Wiley Interscience, New York, 1982, p. 262.
[41] R.N. Rogers, Anal. Chem. 39 (1967) 730–733.
[42] J.C. Dacons, H.G. Adolph, M.J. Kamlet, J. Phys. Chem. 74 (1970) 3035–3040.
[43] M. Kony, I.J. Dagley, D.J. Whelan, J. Phys. Chem. 96 (1992) 8001–8006.
[44] (a) S.A. Shackelford, J.F. Goldman, 203rd Nat. Am. Chem. Soc. Mtg., San Francisco, CA, USA, April 5–10, 1992;
(b) S.A. Shackelford, J.F. Goldman, 22nd International Conference of ICT: Combustion and Reaction Kinetics, Karlsruhe, Germany, July 2–5, 1991.
[45] J.C. Hoffsommer, D.J. Glover, W.L. Elban, J. Energetic Mater. 3 (1985) 149–167.
[46] R. Varga, S. Zeman, J. Hazard. Mater. 132 (2006) 165–170.
[47] To ensure the DNNC-d_6 isotopomer rate constant could be predicted by a y-intercept in graphic Fig. 14, the x-axis had to reflect the number of H-atoms in each isotopomer; so, DNNC-d_6 is represented with 0 H-Atoms on the x-axis. Correspondingly, DNNC-d_4 is (2-H Atoms), DNNC-d_2 (4 H-Atoms), and DNNC (6 H-Atoms).
[48] The y-intercept in Fig. 14 is 0.00477 when carried out to three significant figures even though the Excel-based graph gives this value to only two significant figures (0.0048) as plotted.